# Waveguide-mode polarization gaps in square spiral photonic crystals

Rong-Juan Liu[1,2(a)], Sajeev John[1,3] and Zhi-Yuan Li[2]

[1] *Department of Physics, University of Toronto - 60 St. George St., Toronto, Ontario, M5S1A7 Canada*
[2] *Institute of Physics, Chinese Academy of Sciences - Beijing, 100190 China*
[3] *Department of Physics, King Abdulaziz University - Jeddah, Saudi Arabia*

**Abstract** – We designed waveguide channels in two types of square spiral photonic crystals. Wide polarization gaps, in which only one circular polarization wave is allowed while the other counter-direction circular polarization wave is forbidden, can be opened up on the waveguide modes within the fundamental photonic band gap according to the calculation of band structures and transmission spectra. This phenomenon is ascribed to the chirality of the waveguide and is independent of the chirality of the background photonic crystal. Moreover, the transmission spectra show a good one-way property of the waveguide channels. The chiral quality factor demonstrates the handedness of the allowed and impeded chiral waveguide modes, and further proved the property of the waveguide-mode polarization gap. Such waveguides with waveguide-mode polarization gap are a good candidate for one-way waveguides with robust backscattering-immune transport.

**Introduction.** – A spiral is a type of three-dimensional chiral structure. This kind of structure has attracted much attention because of its optical activity [1–3] and geometric resemblance to the structure of diamonds [4]. Chiral three-dimensional photonic crystals (3D PCs) are an interesting subclass of 3D PCs. Like all photonic crystals, they are famous for having wide complete photonic band gaps (PBGs) [5–8]. In addition to complete PBGs, they can give rise to a special type of band gap due to their structural chirality: polarization gap, in which only one circular polarization wave is allowed to transport in the structure, while the other counter-direction circular polarization wave is forbidden [9–11]. Such polarization stop band gaps have the capability of inducing strong circular dichroism [12–14], which can potentially be used for constructing compact thin-film optical diodes [15].

Recently, Chen *et al.* designed and constructed a one-way waveguide in a layer-by-layer woodpile structure 3D photonic crystal [16]. This waveguide is a chiral waveguide, in which the chiral guided mode is shown to be immune to the scattering from a square patch of metal or dielectric slab inserted to block the channel and exhibits a good one-way property. Interestingly, this one-way waveguide does not result from the breaking of time reversal symmetry (TRS), which plays the central role in one-way waveguides [17–28] built in magneto-optical structures that have been under extensive and intensive studies recently. Instead, it originates from the polarization gap of the chiral waveguide modes, named as waveguide-mode polarization gap (WMPG).

We note that this WMPG is closely related with the chirality only appearing in the waveguide itself. It is a result of the structural chirality of the waveguide. Therefore, it differs from the polarization gap which arises from the structural chirality of the background photonic crystal. In this chiral waveguide, the degeneracy between the left-handed and the right-handed waveguide modes is lifted by the chirality of this waveguide, resulting in a polarization gap when the chirality is strong enough. Suppose that a specific (say, left-handed or right-handed) circularly polarized waveguide mode is the only allowed mode in this gap. When this chiral wave encounters a metal or dielectric slab, the reflected-backward wave will have the same temporal rotational direction as the incident wave since

(a)E-mail: liurj@iphy.ac.cn

no relative phase change occurs in the electric field vector upon reflection. Thus, the reflected circularly polarized wave will have the opposite handedness, namely, the left-handed wave becomes the right-handed wave, or the right-handed wave becomes the left-handed wave, which is forbidden in this WMPG. Therefore, the WMPG guarantees the one-way transport and provides another physical mechanism to construct one-way waveguides in addition to the mechanism of TRS breaking.

A spiral is a natural chiral structure. 3D spiral photonic crystals in different families and with different parameters have different degrees of chirality [6,9]. According to the investigation in ref. [9], the more isolated the spiral units composing the 3D PC are, the more easily the polarization gap comes up. In addition, the overlap of spirals between neighboring lattices will weaken the chirality of the 3D PC. Toader and coworkers [6] proposed two families of square spiral 3D PCs with large complete PBGs. The composing spiral units are well isolated in the [001]-diamond: 1 structure, while strongly overlapped in the [001]-diamond: 5 structure. These two structures are expected to have different degrees of chirality.

In this paper, we designed chiral waveguide channels with polarization gap in [001]-diamond: 1 with strong chirality and [001]-diamond: 5 with weak chirality. The calculated band structures and transmission spectra agree well with each other and show good polarization gap in both structures. We analyze the chiral quality (CQ) factors and find that this quantity well determines the handedness of the only allowed circularly polarization wave in the polarization gaps. Furthermore, we discuss and analyze the influence of the chirality of background photonic crystals on the WMPG, from which we conclude the formation condition of WMPGs.

**Geometrical structures and band structures of perfect [001]-diamond: 1 and [001]-diamond: 5 photonic crystal.** – Figure 1 shows the geometrical structure of the [001]-diamond: 1 and [001]-diamond: 5 photonic crystal. According to the definition in ref. [9], the label $[m1m2m3]$-3D lattice: $n$ spiral is used to denote the family of spiral photonic crystals whose $z$-axis is given by the $[m1m2m3]$ crystallographic axis of a specified 3D lattice. The $n$-th nearest-neighbor points of the 3D lattice are connected via straight segments of dielectric circular rods, forming a 3D spiral structure arm segments. The refractive index of the spiral arms is larger than that of the background medium. We varied the structural parameters to get the optimal structure which can produce large complete PBGs in the background photonic crystals and generate good WMPGs within a photonic crystal waveguide, simultaneously. After many trials and errors, we obtained [001]-diamond: 1 with $[l, c, r, \varepsilon] = [0.72, 1.4, 0.185, 11.9]$ and [001]-diamond: 5 with $[l, c, r, \varepsilon] = [1.6, 1.2, 0.14, 11.9]$, which satisfy our needs. All of the length quantities in this paper are normalized by unit cell size $a$. In $[l, c, r, \varepsilon]$, $l$ is the $xy$-plane
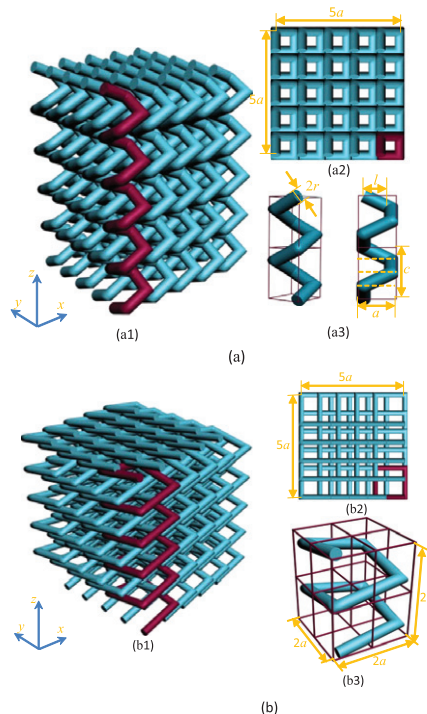


Fig. 1: (Colour on-line) (a) The geometrical structure of [001]-diamond: 1 photonic crystal with $[l, c, r, \varepsilon] = [0.72, 1.4, 0.185, 11.9]$: (a1) the perspective view of a $5 \times 5 \times 5$ supercell, (a2) the top view of a $5 \times 5 \times 5$ supercell, and (a3) the perspective view (left) and the side view (right) of a $1 \times 1 \times 2$ supercell. (b) The geometrical structure of [001]-diamond: 5 photonic crystal with $[l, c, r, \varepsilon] = [1.6, 1.2, 0.14, 11.9]$: (b1) the perspective view of a $5 \times 5 \times 5$ supercell, (b2) the top view of a $5 \times 5 \times 5$ supercell, and (b3) the perspective view of a $2 \times 2 \times 2$ supercell.

projection length of spiral arm between two neighbor elbows, and $c/4$ is the $z$-axis projection length of each spiral arm as shown in fig. 1(a3) and (b3). In a unit cell, the photonic crystal has four spiral arms in four different directions with the same arm length and projection length. $r$ is the radius of cylindrical arm rods, whose dielectric constant is $\varepsilon$. $\varepsilon = 11.9$ is adopted in this paper, corresponding to the material of silicon in the infrared regime. The length of an arm rod between two neighbor elbows equals $\sqrt{l^2 + c^2}$, the height in the $z$-direction of a unit cell equals $c$, and the $x(y)$ side length of a unit cell is equal to $a$. For the [001]-diamond: 1 photonic crystal, the spirals overlap a little bit between neighbor cells because of the relatively big radius, as shown in fig. 1(a). From the top view in fig. 1(a2), we can see that each spiral is nearly contained within its own unit cell and isolated from the neighbor cells (with only a little bit overlap with other spirals). This geometry will result in a relatively strong chirality. For the [001]-diamond: 5 photonic crystal, because $l = 1.6$ is larger than the $x(y)$ side length (normalized as 1) in a unit cell, the spiral arms stride over two neighbor cells as shown in fig. 1(b3) and lead to a big overlap of
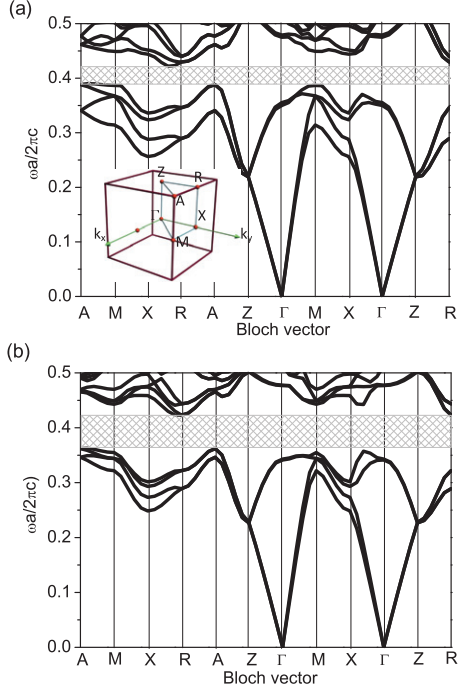
Fig. 2: (Colour on-line) (a) Calculated band structure of the [001]-diamond: 1 photonic crystal with $[l, c, r, \varepsilon] = [0.72, 1.4, 0.185, 11.9]$; (b) calculated band structure of the [001]-diamond: 5 photonic crystal with $[l, c, r, \varepsilon] = [1.6, 1.2, 0.14, 11.9]$.

neighbor spirals (see fig. 1(b1) and (b2)), so the chirality is weak.

We first investigate the basic optical properties of these two chiral photonic crystal structures, and find that they both have complete PBGs lying between the 4th and 5th bands, according to the band diagrams displayed in fig. 2. We calculate the band structure by using the open source software MPB package that is based on the plane wave expansion method and released by Steven Johnson in MIT [29]. In the calculation, the mesh-grid point number is 32 in a unit length 1. Figure 2(a) shows the band structure of the [001]-diamond: 1 photonic crystal with $[l, c, r, \varepsilon] = [0.72, 1.4, 0.185, 11.9]$. The frequency range of the complete PBG is 0.390–0.422, while the directional band gap in the $z$-direction (namely, the $\Gamma Z$-direction) is in the range 0.355–0.479. Figure 2(b) shows the band structure of the [001]-diamond: 5 photonic crystal with $[l, c, r, \varepsilon] = [1.6, 1.2, 0.14, 11.9]$. The complete PBG is located in the range 0.362–0.423, and the directional band gap in the $z$-direction is in the range 0.355–0.476.

**Waveguide modes in [001]-diamond: 1 photonic crystals.** – We construct a waveguide in [001]-diamond: 1 with $[l, c, r, \varepsilon] = [0.72, 1.4, 0.185, 11.9]$ by removing a coil of spiral along the $z$-axis direction, as shown in fig. 3. The transmission spectrum in fig. 4(a) and the corresponding band structure in fig. 4(b) show that the waveguide exhibits good WMPGs in the fundamental
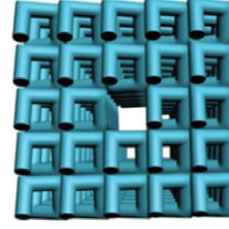


Fig. 3: (Colour on-line) The geometric structure of waveguide in a [001]-diamond: 1 photonic crystal with $[l, c, r, \varepsilon] = [0.72, 1.4, 0.185, 11.9]$, which is generated by removing a whole coil of spiral along the $z$-axis direction.
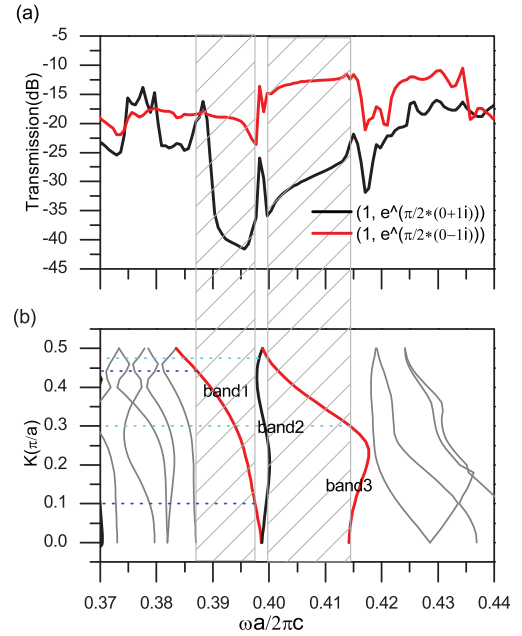


Fig. 4: (Colour on-line) Calculated transmission spectrum (a) and the corresponding band diagram structure (b) for the waveguide created in a [001]-diamond: 1 photonic crystal with $[l, c, r, \varepsilon] = [0.72, 1.4, 0.185, 11.9]$, as shown in fig. 3. The black curve in (a) is the transmission spectra with the incident source $(E_x, E_y)$ polarized as $(1, e^{\frac{\pi(0+1i)}{2}})$, and the red curve is for the incident source $(E_x, E_y)$ polarized as $(1, e^{\frac{\pi(0-1i)}{2}})$. The shadow regions are two WMPGs.

complete PBG. The band structure is also calculated by using MPB, while the transmission spectrum is calculated by using MEEP [30], also released by MIT, with the same mesh-grid point number as in the MPB calculation. In the calculation of transmission spectrum, we set two counter-direction circularly polarized incident light sources. In order to get these two incident lights, we set the initial amplitude of the $E$-field components $(E_x, E_y)$ as $(1, e^{\frac{\pi(0+1i)}{2}})$ for one circularly polarized wave and $(1, e^{\frac{\pi(0-1i)}{2}})$ for the inverse circularly polarized wave. Along the waveguide direction ($z$-axis direction), we set perfect matching layers (PMLs) at the two sides of the waveguide. At the directions perpendicular to the waveguide ($x(y)$ direction),
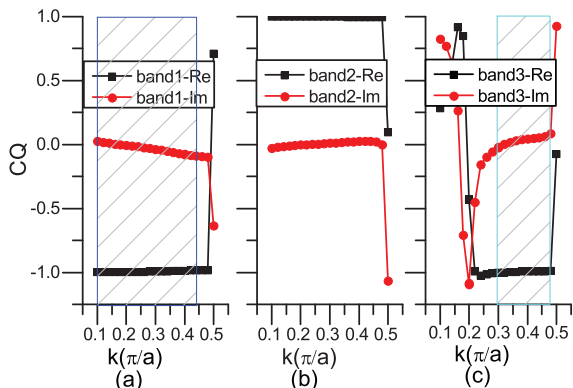
Fig. 5: (Colour on-line) The CQ factors for (a) band 1, (b) band 2, and (c) band 3. The red and black dotted lines correspond to the real and imaginary part of CQ, respectively. The shadow regions correspond to the WMPGs band.
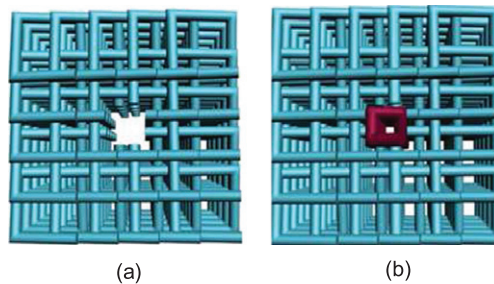


Fig. 6: (Colour on-line) The geometric structures of waveguide in the [001]-diamond: 5 photonic crystal with background spiral parameters of $[l, c, r, \varepsilon] = [1.6,\ 1.2,\ 0.14,\ 11.9]$. (a) The waveguide structure formed by drill a cubic block air hole; (b) the waveguide structure formed by inserting a new spiral with parameters of $[l_w, c_w, r_w, \varepsilon_w] = [0.7,\ 1.2,\ 0.16,\ 15]$ into the air hole in (a).

we used the periodic boundary condition and the supercell technique with $5 \times 5$ cells. The supercell technique is also adopted in the band diagram calculation. Figure 4(b) shows that there are three waveguide modes in the fundamental complete PBG named as band 1, band 2, and band 3. Combining the corresponding transmission spectra with the band structure, we can see that there are two broadband WMPGs ranging within 0.389–0.398 and 0.400–0.414. They are located within band 1 and band 3, respectively. In both of these two polarization gaps, the red curve polarized as $(1, e^{\frac{\pi(0-1i)}{2}})$ shows higher transmission efficiency. The difference between the transmission efficiencies of these two circular polarized waves can reach about 20 dB for both band 1 and band 3, which means one polarization wave is allowed and the other is forbidden. It seems that band 1 and band 3 have the same handedness and band 2 has an inverse handedness. In order to make sure of this, we calculated the CQ factors of the three waveguide modes shown in fig. 5. As described in refs. [9] and [22], the CQ factor is defined as $CQ = \frac{\langle E_x \rangle}{i \langle E_y \rangle}$, where $\langle \cdots \rangle$ is the spatial average over a cubic unit cell, and $E_x$ and $E_y$ are the $x$ and $y$ components of the electric field. It can effectively characterize the direction of the temporal rotation of the electric field. It is a complex number. When $CQ = 1 + 0i$, the electric field vector rotates clockwise as time goes by, as seen against the positive $z$-axis direction. When $CQ = -1 + 0i$, the electric field vector rotates anticlockwise against the positive $z$-axis direction. If CQ deviates from $\pm 1$, it indicates the guided mode becomes elliptically polarized. We calculated the $E_x$ and $E_y$ components using MPB, obtained their 3D distribution profiles within a unit cell, and calculated the corresponding values of $\langle E_x \rangle$ and $\langle E_y \rangle$, and then the CQ factor. Figures 5(a), (b) and (c) show the real part and imaginary part of the CQ factors for the three bands: band 1, band 2, and band 3, respectively. From the real part and imaginary part, we find that band 1 in the $k$-point range $(0$–$0.5)\frac{\pi}{a}$ and band 3 in the $k$-point range

$(0.3$–$0.5)\frac{\pi}{a}$ have the same factor $CQ = -1 + 0i$ indicating anticlockwise circular rotation of electric field, and band 2 in the $k$-point range $(0$–$0.5)\frac{\pi}{a}$ has the inverse factor and the inverse rotation, namely, the clockwise rotation. These characteristics of CQ factors agree with the characteristics of the transmission spectra.

Band 1 and band 2 keep good chirality in the whole Brillouin zone except at its edge, while band 3 only keeps good chirality for $k \geq 0.3\frac{\pi}{a}$. The shadow regions on band 1 (fig. 5(a)) and band 3 (fig. 5(c)) are the corresponding regions of WMPGs. For band 1, the $k$-point range $(0.1$–$0.44)\frac{\pi}{a}$ in fig. 5(a) covers the frequency range $(0.387$–$0.397)\frac{2\pi c}{a}$ in fig. 4; for band 3, the $k$-point range $(0.3$–$0.49)\frac{\pi}{a}$ in fig. 5(c) corresponds to the frequency range $(0.399$–$0.414)\frac{2\pi c}{a}$ in fig. 4. In band structure the WMPG regions are the single-mode region with monotonous slope. Otherwise, at the edge of the Brillouin zone, it presents extraordinary chiral behavior. This has been explained in ref. [11] according to the chiral resonance condition. For circular polarization of light, the tip of the electric field vector simply follows a spiral. The pitch of this spiral is just the material wavelength $\lambda$. Thus, intuitively, we expect a chiral resonance if the pitch of circularly polarized light matches the pitch of the dielectric spiral, *i.e.*, the lattice constant in the $z$-direction $a_z$. The condition $\frac{\lambda}{a_z} = 1$ corresponds to the edge of the second Brillouin zone, *i.e.*, to a wave number $k_z = \frac{2\pi}{\lambda} = \frac{2\pi}{a_z}$. However, the edge of the first Brillouin zone is lying at $k_z = \frac{\pi}{a_z}$. One does not anticipate a strong chiral response around and below the fundamental stop band (or band gap), but rather at higher frequencies.

**Waveguide modes in [001]-diamond: 5 photonic crystal.** – We construct a waveguide in the [001]-diamond: 5 photonic crystal with $[l, c, r, \varepsilon] = [1.6,\ 1.2,\ 0.14,\ 11.9]$ by removing a chain of cubic unit cell along the $z$-axis direction, leaving an air block with the size of $1 \times 1 \times \infty$ (fig. 6(a)), and then inserting a new spiral different from the spirals composing
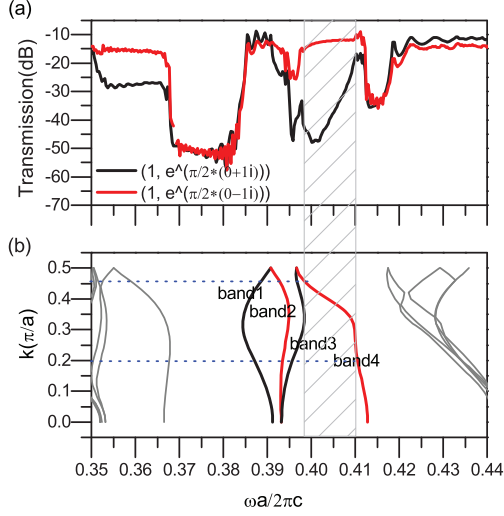
Fig. 7: (Colour on-line) (a) The transmission spectrum of waveguide [001]-diamond: 5 shown in fig. 6 and (b) the corresponding band structure. The black curve is the transmission spectra with incident source $(E_x, E_y)$ equal to $(1, e^{\frac{\pi(0+1i)}{2}})$, and the red curve is with incident source $(E_x, E_y)$ equal to $(1, e^{\frac{\pi(0-1i)}{2}})$.
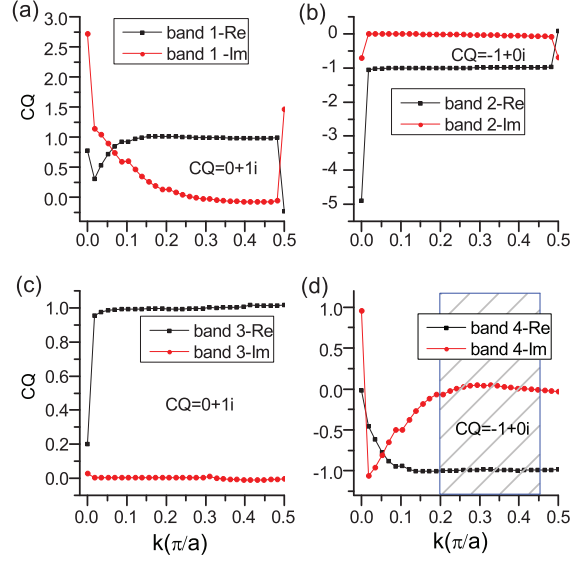


Fig. 8: (Colour on-line) The CQ factors for (a) band 1, (b) band 2, (c) band 3, and (d) band 4. The red dotted line is the real part of CQ, and the black dotted line is the corresponding imaginary part. The shadow region is the WMPG region.

the background square spiral photonic crystal as shown in fig. 6(b). As in the case of the [001]-diamond: 1 photonic crystal, by adjusting the structural parameters, we obtain good WMPGs in the fundamental complete PBG when $[l, c, r, \varepsilon] = [1.6, 1.2, 0.14, 11.9]$ and the new spiral inserted in the waveguide has parameters of $[l_w, c_w, r_w, \varepsilon_w] = [0.7, 1.2, 0.16, 15]$. In determining the structural parameters by increasing $l_w$ from 0 to 0.7 (when $l_w = 0$, it is a straight rod), we found that the stronger the chirality (the bigger ratio of $l_w : c_w$) of the inserted spiral, the better the WMPG is. Figures 7(a) and (b) show the transmission spectrum and the corresponding band structure of the waveguide. There are 4 waveguide modes present within the fundamental complete PBG. Looking at the transmission spectra, we can see that only band 4 in the frequency range $(0.397\text{--}0.41)\frac{2\pi c}{a}$ exhibits good WMPG. In this gap, the difference between the transmission efficiency for two inverse polarized waves is about 30 dB. This clearly indicates that only one circularly polarized wave is allowed to propagate through the waveguide channel and the waveguide shows good one-way property.

The CQ factors for the four waveguide modes are shown in fig. 8. It can be seen that band 1 and band 3 in the main Brillouin zone have the same handedness ($CQ = 1 + 0i$), while band 2 and band 4 have the same handedness ($CQ = -1 + 0i$). Although all these 4 bands possess good handedness in considerable $k$-point regions, especially band 2 and band 3, not all of them generate good WMPGs. The parabolic dispersion curve property of band 1 leads to the passage of both circularly polarized waves with counter-direction, and the point of inflexion on band

1 in fig. 7(b) causes the changing of handedness as reflected in the variation of the CQ in fig. 8(a), therefore no WMPG is generated. Band 2 and band 3 have almost perfect handedness, but they do not show good WMPG either, because of their counter-direction circular polarization and the offset of handedness in their overlapping region.

**Conclusion.** – We have investigated WMPGs in the relatively strong chiral structure [001]-diamond: 1 photonic crystal with $[l, c, r, \varepsilon] = [0.72, 1.4, 0.185, 11.9]$ and the weak chiral structure [001]-diamond: 5 photonic crystal with $[l, c, r, \varepsilon] = [1.6, 1.2, 0.14, 11.9]$. We have found that no matter how strongly chiral the background photonic crystal is, a WMPG is available by setting a waveguide channel with strong chirality. For the case of [001]-diamond: 1 photonic crystal with $[l, c, r, \varepsilon] = [0.72, 1.4, 0.185, 11.9]$, simply removing a coil of spiral results in large frequency ranges of WMPG. This result is not ascribed to the strong chirality of the background photonic crystal, but to the essentially strong chirality of the waveguide channel itself. This point has been further proved by the case of [001]-diamond: 5 photonic crystal with $[l, c, r, \varepsilon] = [1.6, 1.2, 0.14, 11.9]$. [001]-diamond: 5 photonic crystal has weak chirality due to strong overlap. It only provides a photonic crystal background with complete PBG to confine the waveguide mode. When drilling a cubic air hole in the photonic crystal along the chiral axis direction, this channel itself also has weak chirality which supports two counter-directional circularly polarized waves. Therefore, no WMPG exists. In comparison, when a new spiral is inserted in this channel, the chirality of this channel is changed by this spiral from weak to strong and

leads to a WMPG. Moreover, the stronger the inserted spirals chirality is, the better the polarization gap is.

Recently, one-way waveguides with topologically protected robust transport behavior characterized by robust backscattering-immune transport have become a hot topic [17–28]. Our WMPGs designed in these two square spiral photonic crystals also provide a foundation for such a one-way waveguide. In a WMPG, only one kind of circularly polarized waveguide mode is allowed to propagate. For a pair of counter-propagating chiral modes with the same handedness, their coupling is suppressed as the temporal rotation of the electric field at a given point in space has opposite directions. Thus, when a circularly polarized wave encounters a metal or dielectric obstacle, the reflected backward wave will have the same temporal rotational direction. Therefore, the reflected circularly polarized wave will have the opposite handedness which is forbidden in the channel. The backscattering-immune transport is maintained.

$$* * *$$

## REFERENCES

[1] Tinoco I. and Freeman M. P., *J. Phys. Chem.*, **61** (1957) 1196.

[2] Brown P. J. and Forsyth J. B., *Acta Crystallogr.*, **A52** (1996) 408.

[3] Shadrivov I. V., *Appl. Phys. Lett.*, **101** (2012) 041911.

[4] Chutinan A. and Noda S., *Phys. Rev. B*, **57** (1998) 2006.

[5] Toader O. and John S., *Science*, **292** (2001) 1133.

[6] Toader O. and John S., *Phys. Rev. E*, **66** (2002) 016610.

[7] Kennedy S. R., Brett M. J., Toader O. and John S., *Photon. Nanostruct. - Fundam. Appl.*, **1** (2003) 37.

[8] Kennedy S. R., Brett M. J., Toader O. and John S., *Nano Lett.*, **2** (2002) 59.

[9] Lee J. C. W. and Chan C. T., *Opt. Express*, **13** (2005) 8083.

[10] Thiel M., Fischer H., Freymann G. V. and Wegener M., *Opt. Lett.*, **35** (2010) 166.

[11] Thiel M., Decker M., Deubel M., Wegener M., Linden S. and Freymann G. V., *Adv. Mater.*, **19** (2007) 207.

[12] Hrudey P. C. P., Szeto B. and Brett M. J., *Appl. Phys. Lett.*, **88** (2006) 251106.

[13] Mitov M. and Dassaud N., *Nat. Mater.*, **5** (2006) 361.

[14] Furumi S. and Sakka Y., *Adv. Mater.*, **18** (2006) 775.

[15] Hwang J., Song M. H., Park B., Nishimura S., Toyooka T., Wu J. W., Takanishi Y., Ishikawa K. and Takezoe H., *Nat. Mater.*, **4** (2005) 383.

[16] Chen W.-J., Hang Z. H., Dong J.-W., Xiao X., Wang H.-Z. and Chan C. T., *Phys. Rev. Lett.*, **107** (2011) 023901.

[17] Haldane F. D. M. and Raghu S., *Phys. Rev. Lett.*, **100** (2008) 013904.

[18] Wang Z., Chong Y. D., Joannopoulos J. D. and Soljacic M., *Phys. Rev. Lett.*, **100** (2008) 013905.

[19] Ao X. Y., Lin Z. and Chan C. T., *Phys. Rev. B*, **80** (2009) 033105.

[20] Wang Z., Chong Y. D., Joannopoulos J. D. and Soljacic M., *Nature (London)*, **461** (2009) 772.

[21] Fu J.-X., Liu R.-J. and Li Z.-Y., *Appl. Phys. Lett.*, **97** (2010) 041112.

[22] Fu J.-X., Liu R.-J., Gan L. and Li Z.-Y., *EPL*, **93** (2010) 24001.

[23] Fu J.-X., Liu R.-J. and Li Z.-Y., *EPL*, **89** (2010) 64003.

[24] Fu J.-X., Lian J., Liu R.-J., Gan L. and Li Z.-Y., *Appl. Phys. Lett.*, **98** (2011) 211104.

[25] Poo Y., Wu R. X., Lin Z. F., Yang Y. and Chan C. T., *Phys. Rev. Lett.*, **106** (2011) 093903.

[26] Shen J., Liu S. Y., Zhang H. W., Chui S. T., Lin Z. F., Fan X., Kou X. M., Lu Q. and Xiao J. Q., *Plasmonics*, **7** (2012) 287.

[27] Yang Y., Poo Y., Wu R. X., Gu Y. and Chen P., *Appl. Phys. Lett.*, **102** (2013) 231113.

[28] Skirlo S. A., Lu L. and Soljačić M., *Phys. Rev. Lett.*, **113** (2014) 113904.

[29] http://ab-initio.mit.edu/wiki/index.php/MIT_Photonic_Bands.

[30] http://ab-initio.mit.edu/wiki/index.php/Meep.